UNCLASSIFIED
(Approved for publication)

CLM - P 11

VACUUM ULTRA-VIOLET RADIATION FROM A MAGNETICALLY COMPRESSED PLASMA

By

A.H. GABRIEL, G.B.F. NIBLETT and N.J. PEACOCK

Submitted for publication in Journal of Quantitative Spectroscopy and Radiative Transfer.

U.K.A.E.A. Research Group,
Culham Laboratory,
Abingdon,
Berks.

July, 1962

VACUUM ULTRA-VIOLET RADIATION FROM A MAGNETICALLY COMPRESSED PLASMA

A.H. Gabriel
G.B.F. Niblett
N.J. Peacock

Abstract

In recent years there has been an increasing interest in the production of energetic plasmas at temperatures and densities relevant to the study of controlled thermonuclear reactions. Experiments of this type at AWRE Aldermaston use rapidly rising axial magnetic fields to ionise and compress deuterium gas to particle densities in excess of $10^{17} cm^{-3}$ and temperature approaching 10^7 °K. A megajoule condenser bank under construction is designed to increase these densities and temperatures, and extend the duration of the discharge to tens of microseconds. Such a plasma provides a controlled laboratory source of electromagnetic radiation whose energy peaks in the vacuum ultra-violet and soft X-ray spectral regions. Production of such a plasma stimulates the study of radiative processes in this energy range, and requires the development of vacuum ultra-violet and X-ray instruments for measuring its properties.

This paper reviews the characteristics of radiation emitted by hydrogenic plasma at a particle density of 10^{17} cm^{-3} and temperature of 10^7 °K containing a small admixture of oxygen and permeated with an axial magnetic field of some 50 kilogauss. The distribution of the ionic species in steady state conditions is discussed and the contribution of free-free, free-bound and bound-bound transitions to the radiation spectrum is evaluated. Phenomena such as stark broadening, doppler shifts, and zeeman splitting are considered as physical processes which can be used to diagnose the state of the plasma.

The final section of the paper describes the experimental programme of vacuum ultra-violet radiation measurements in

progress at AWRE. Soft X-ray pin-hole camera photographs have been used to establish the dimensions of the emitting plasma and absorption measurements using aluminium, beryllium, carbon and nickel foils have provided estimates of the electron temperature from the short wave-length spectral cut-off. Several new instruments constructed at the establishment will shortly be available for studying the vacuum spectrum of the plasma. These include: a versatile X-ray crystal spectrometer; a grazing incidence spectrograph available with photoelectric recording; and a photographic instrument which uses a concave grating at near normal incidence and which is time-resolved by reflection at 70° from a high speed rotor. Preliminary results obtained with this latter instrument are briefly discussed.

TABLE OF CONTENTS

1. INTRODUCTION

The last decade has witnessed remarkable advances in the production of highly ionised gases at elevated temperatures and densities. Whereas 10 years ago the establishment of a plasma at a temperature of 10^5 ^{o}K was exceptional, recent experiments, largely motivated by the quest for a controlled thermonuclear reactor, have demonstrated the feasibility of generating within a few microseconds plasma with electron temperatures of 10^7 ^{o}K at particle densities in excess of 10^{17} cm^{-3}. The formation of plasmas whose electrons have mean thermal energies of a kilovolt results in copious electromagnetic radiation whose energy peaks at wave-lengths between 1 Å and 100 Å i.e., in the vacuum ultra-violet and soft X-ray spectral regions. Thus for thermonuclear experiments the study of radiative processes at these wave-lengths becomes of great importance not only because such radiation constitutes the dominant cooling mechanism but also because the analysis of its spectrum is a valuable means of diagnosing the state of the plasma without introducing a perturbation. Likewise the existence of plasmas at these high temperatures prompts the design of instruments for studying energetic radiative processes; the radiating plasma is of great value as a controlled laboratory light source.

The present paper describes briefly the type of magnetic compression experiment which is being studied at AWRE, Aldermaston, and which currently produces deuterium plasmas with ion and electron temperatures of several hundred eV. It then surveys the principal characteristics of vacuum ultra-violet radiation from such a dense hot plasma and summarises the programme of vacuum ultra-violet and soft X-ray measurements which is now under way.

2. THE MAGNETIC COMPRESSION EXPERIMENT

The rapid magnetic compression of plasmas using axial magnetic fields, or the θ-pinch as this type of discharge is commonly called, is currently being studied in many plasma physics laboratories throughout the world of which the most notable include the Scylla experiment at Los Alamos (1) and a similar experiment at N.R.L. (2). At AWRE the fast-rising magnetic field is produced by the application of a low inductance condenser bank to a single-turn coil 20 cm long and 5 cm in diameter which encircles a length of alumina or quartz tube of internal diameter 4 cm. The Maggi I condenser bank, shown schematically in Figure 1, has been used for the radiation measurements;

it stores 45 kJ of electrical energy at 30 kV in a circuit whose total inductance including the coil gives a half-period of 4 μs. The bank is switched on to the coil by 200 parallel spark gaps and with the coil shown in Figure 1 the peak current is 2×10^6 A and the peak field 100 kilogauss.

Using initially un-ionised deuterium gas at 100 μ pressure the discharge consists of about 5 or 6 half-cycles of which the second is observed to yield the highest gas temperatures and gas purity. On the first half-cycle the plasma is only weakly diamagnetic and serves to provide the necessary pre-ionisation for the second half-cycle whilst the third and subsequent half-cycles are increasing contaminated by impurity atoms from the wall.

The temperature and densities attained on the second half-cycle depend primarily on the sign and magnitude of the magnetic field which is trapped and compressed within the plasma and this in turn is a sensitive function of initial pressure. The highest temperatures occur when the initial pressure is in the neighbourhood of 100 μ when the trapped field is reversed with respect to the external field. The complex mechanisms by which the trapped reversed field heats the plasma consist essentially of two processes: firstly, dynamic effects in which high energies are imparted to the plasma ions by the tensions in the reversed magnetic field lines as they encircle the plasma and pull it to the centre of the coil; and secondly, a rapid resistive heating of the electrons derived from high field gradients and current densities which are maintained across the plasma by the trapped reversed field. Limited data from experiments in which long coils are used (3) suggest that under these conditions the dynamic motion is much less important than field diffusion so that the ion and electron temperatures can be explained adequately in terms of resistive heating alone.

AWRE experiments using the circuit shown in Figure 1 yield at peak field on the second half-cycle a plasma which is kept well away from the walls by magnetic confinement and has a well-defined sharp boundary. A variety of measurements show that under optimum conditions the peak electron temperature is 400 eV and the peak ion temperature (known much less precisely) about 700 eV. Absolute measurements of the radiation in the visible continuum are consistent with a deuterium plasma of peak density 10^{17} cm^{-3} contaminated with 1% of oxygen. At present the 4μs half-cycle is limited by the energy stored in the condenser bank. A fast megajoule condenser bank which will be completed at the Culham laboratory early in 1963 will extend

this time to tens of microseconds and use coils up to 3 metres long. It is predicted that this larger experiment will produce plasmas of over 10^{7} °K at densities much in excess of 10^{17} cm^{-3}.

3. RADIATION FROM A DENSE HOT PLASMA

In this section we outline the principal features of the radiation from a plasma produced in the θ-pinch and in particular we are concerned to show how the various features can be used to yield information on the plasma state. To fix our ideas we consider the radiation from 1 c.c. of deuterium plasma at a temperature of 10^{7} °K and particle density of 10^{17} cm^{-3} containing 1% oxygen and permeated with a trapped field of 50 kilogauss. In order to simplify the discussion we assume that the time-scale is long enough for this plasma to reach a steady state.

The spectral distribution of the radiation from a black body at temperature T is given by the Planck function,

$$j_{\lambda} = \frac{2hc^{2}\lambda^{-5}}{\left[e^{(hc/\lambda kT)}-1\right]} \text{ erg cm}^{-2}\text{ s}^{-1}\text{ steradian}^{-1}\text{ cm}^{-1} \qquad \ldots.(1)$$

where j_{λ} is the intensity per unit wave-length and the other symbols have their customary meaning. This relationship is plotted in Figure 2 for T = 10^{7} °K and reaches a peak value at 3 Å. For our densities and dimensions the plasma does not of course radiate as a black body (if it did its characteristic cooling time would be 10^{-15} s), but the Planck curve is nevertheless of interest since for a thermal plasma it determines the maximum radiation possible at any wave-length

For a transparent plasma the radiation spectrum is composed of continuum with superimposed line radiation and in order to discuss the contribution these make, it is necessary to consider the equilibrium population of ionic states. In complete thermodynamic equilibrium the relative population of ionic states is governed by the Saha expression which implies a detailed balance between all the various radiative and collisional processes and leads to an ionization equation which is density dependent, giving a higher degree of ionization the lower the density. However, in a low density plasma whose dimensions are such

that the radiation escapes, the ionization state is determined by a balance between radiative processes at the low effective radiation temperature and collision processes at high kinetic temperature. Such an ionization equation, e.g., that developed for the sun's corona, and discussed by Woolley and Stibbs (4) and in greater detail by Elwert (5), involves limited balance between photoelectric recombination and collisional ionization which are both two-body processes, and thus yield an equilibrium independent of density. At the conditions we have specified, the ionization equilibrium is determined by this type of limited balance. The deuterium is of course fully ionized and calculations show that the oxygen atoms are stripped down to the last electron with the population of OVIII, compared with OIX at about 1%. Assuming this ionic distribution, it is possible to plot the contributions of free-free, free-bound and bound-bound transitions to the radiation spectrum.

3.1 Bremsstrahlung radiation

It is necessary to consider only electron-ion bremsstrahlung since electron-electron quadrupole emission exists only for relativistic electrons and is negligible at $10^7\ ^{o}K$. The free-free radiant flux from a plasma with ion and electron densities N_i and N_e at an electron temperature T_e and nuclear charge Z can be written (6),

$$j_{\lambda}^{f-f} = A \frac{g N_e N_i Z^2}{(kT)^{1/2}} \frac{1}{\lambda^2} e^{-(hc/kT\lambda)} \text{ erg cm}^{-3} \text{ s}^{-1} \text{ steradian}^{-1} \text{ cm}^{-1} \quad \ldots\ldots(2)$$

In this expression A is a constant term $\frac{16}{3}\left(\frac{\pi}{6m_e^3}\right)^{1/2}\frac{e^6}{c^2}$

whose numerical value is 1.91×10^{-36}. The term g is the gaunt factor which expresses the quantum mechanical departure from Kramer's classical calculation and is approximately equal to unity at short wavelengths (less than 10^{-5} cm) but increases to five in the far infra-red. The bremsstrahlung curve for pure deuterium is plotted in Figure 2 and, allowing for self-absorption and stimulated emission at long wave lengths, defines the minimum radiation from a plasma with T_e of $10^{7\ o}K$ and N of $10^{17}\ cm^{-3}$. The curve has its maximum in the far

vacuum ultra-violet at 7 Å. High Z impurities increase the bremsstrahlung radiation significantly because of the Z^2 dependence on nuclear charge and the effect of 1% of oxygen is included as a separate curve in Figure 2.

At long wave-lengths such as the visible the bremsstrahlung curve exhibits the usual $\frac{1}{\lambda^2}$ dependence but at short wave-lengths there is a rapid exponential drop in intensity. This short wave-length cutt-off has formed the basis of measurements of electron temperature from absorption measurements using thin foils (7)(8) and from crystal spectrometer analysis of the continuum (9).

3.2 Recombination Radiation

This is somewhat more complicated than bremmsstrahlung to evaluate since it varies markedly from one ion to another. However, for the special case of hydrogen-like ions the expression can be written (6)

$$j^{f-b}_{\lambda,n} = \frac{4\pi^2 e^4}{h^2} m_e A f \frac{N_e N_i q Z^4}{(kT_e)^{3/2}} \frac{1}{n^3} \frac{1}{\lambda^2} e^{\left(\frac{hc}{kT}\right)\left(\frac{1}{\lambda_n} - \frac{1}{\lambda}\right)} \text{ erg cm}^{-3} \text{ s}^{-1} \text{ steradian}^{-1} \text{ cm}^{-1} \quad \ldots.(3)$$

where A is the same constant as for bremsstrahlung, f is the recombination gaunt factor and q is the fractional abundance of the ionization state considered. The term $j^{f-b}_{\lambda,n}$ is the intensity of recombination radiation from the continuum to the bound state with principal quantum number n and λ_n is the wave-length of the series limit. At any particular wave-length it is necessary to sum up the contribution from all the various series limits. Equation (3) shows that for a given electron temperature the shape of the recombination continuum is the same as for bremsstrahlung even though the absolute values may be markedly different, so that as long as measurements are made at wave-lengths shorter than the series limit the presence of recombination radiation does not preclude determinations which depend on the shape of the continuum (8)(9). The electron temperature may also be measured from the increase in intensity at the series limit since from equations (2) and (3) the ratio is given by

$$\frac{j^{f-b}_{\lambda,n}}{j^{f-f}_{\lambda}} = \frac{4\pi^2 e^4 m_e}{h^2} \frac{fg}{g} \frac{Z^2}{(kT_e)} \frac{1}{n^3} e^{hc/kT\lambda_n} \quad \ldots.(4)$$

giving a determination of temperature which is independent of the density but requires a knowledge of the impurity content.

For deuterium the Lyman α series limit is at 912 Å and at an ion density of 10^{17} cm^{-3} would be broadened to a width of about 25 Å by the inter-ionic electric fields. However at 10^7 °K the contribution of recombination radiation beyond this series limit is negligible and all the recombination radiation comes from impurity ions. Figure 2 includes the contribution to be expected from hydrogen-like OVIII beyond the Lyman edge at 14.2 Å.

3.3 Line Radiation

The importance of line radiation as a source of energy loss from high temperature plasma has been emphasised by many authors particularly Knorr (10) and Post (11). General analytical expressions for line radiation tend to be clumsy since the intensity varies strongly with the transition. However, in a deuterium discharge at 10^7 °K the hydrogen-like OVIII ions which are present would radiate strongly in the Lyman α resonance line at 19 Å and for such an ion the radiation intensity can be written in the form

$$\int_{line} j_\lambda d_\lambda = \frac{1}{4\pi} \frac{hc}{\lambda} \frac{A_{m,n}}{\sum A_m} qN_i N_e \langle \sigma v_e \rangle \quad \ldots.(5)$$

which expresses the balance between electron excitation and radiative decay for conditions of limited balance. In this equation $A_{m,n}$ is the transition probability, the summation is for all transitions from state m, σ is the excitation cross-section for electrons of velocity v_e and the brackets indicate an average taken over the electron velocity distribution.

3.4 Line Broadening

It is important to note how the various line broadening mechanisms vary with wave-length in the vacuum ultra-violet region. The relevant processes are doppler broadening and zeeman splitting.

Doppler broadening of a spectral line emitted by an assembly of ions with a maxwellian velocity distribution at a temperature T_i is given by

$$\Delta\lambda_D = 0.85 \frac{\lambda}{c} \sqrt{\frac{2kT_i}{m_i}} \qquad \ldots.(6)$$

where $2\Delta\lambda_D$ is the half width and m_i the ion mass. Thus the doppler width is proportional to the wave-length and for oxygen at 10^7 ^oK the width for $\lambda = 20$ Å is about 0.01 Å. A proposal to measure doppler widths of X-ray lines has been made by the Scylla team (12) who note that the doppler effect is the most important source of line broadening at short wave-lengths.

The stark broadening of emission lines of ions in a high temperature plasma is more difficult to analyse since it depends strongly on the transition concerned. However, for hydrogen-like ions such as OVIII which all have a linear stark effect Unsold gives an approximate expression in the form

$$\Delta\lambda_s \sim \frac{0.01\lambda^2 n^2 F_o}{Z} \qquad \ldots.(7)$$

where λ is in centimetres, n is the principal quantum number of the upper level of the transition and F_o is the normal electric field strength defined as the strength at the mean distance between neighbouring particles and is given by $F_o = 2.6\ e\ N_i^{2/3}$ in electrostatic units. We see that stark broadening decreases more rapidly with decreasing wave-length than the doppler broadening so that in the soft X-ray region the effect is not measurable.

The zeeman splitting of spectral lines is a possible method of measuring the strength and polarity of trapped magnetic fields and leads to a determination of the plasma β. The expression for zeeman splitting is

$$\Delta\lambda_z = gL\lambda^2 H \qquad \ldots\ldots (8)$$

where λ is again in centimetres, L is the Lorentz term $\frac{e}{4\pi m_e c^2}$ with numerical value 4.7×10^{-5} and H is the field strength in gauss. Thus with a Lande g factor of unity the expression becomes

$$\Delta\lambda_z = 4.7\ 10^{-5}\lambda^2 H$$

again showing the λ^2 dependence of the line splitting. The technique is therefore only possible at long wave-lengths since for $\lambda = 1000$ Å and H = 50 kilogauss, $\Delta\lambda_z = 0.025$ Å. To measure this small splitting in the presence of broadening by other processes requires specialised equipment and since wave-lengths of the order of 1000 Å are necessary the measurement is not of great interest for temperatures which approach 10^7 °K.

4. CURRENT EXPERIMENTAL PROGRAMME

Measurements of the visible spectrum on the first half-cycle of our present discharge show a low temperature plasma (~ 5 eV) emitting balmer lines against a background continuum with oxygen as the only impurity. On the second half-cycle the continuum radiation in the visible follows closely a $\frac{1}{\lambda^2}$ dependence and absolute intensity measurements at 3800 Å are consistent with a peak particle density of 10^{17} cm^{-3} and an oxygen content of 1% by atoms.

4.1 Soft X-ray Absorption Measurements

The electron temperature on the second half-cycle has been measured from the shape of the spectral curve at low wave-lengths where the radiation intensity falls off rapidly with decreasing wave-length. Pin-hole camera photographs of the plasma in the soft X-ray region taken by filtering the radiation through a thin aluminium

absorber mounted on melinex film are shown in Figure 3 which also illustrates the time-dependence of the radiation recorded with a scintillation detector. The pin-hole photographs serve to establish the radial dimensions of the emitting plasma and confirm that the hot gas is confined well away from the tube walls. There is satisfactory agreement between the radius of the plasma measured from X-ray emission and that determined from high speed cameras using visible radiation.

The electron temperature has been estimated from scintillator measurements of the transmission through varying thicknesses of each of four different types of material: aluminium, beryllium, carbon and nickel. The relative transmission was taken from the peak pulse height and pulse area of the scintillator output averaged over 20 shots for each material. The measurements have been compared with the theoretical transmission of a bremsstrahlung continuum as computed from the appropriate absorption cross-sections and typical results using carbon foils are shown in Figure 4. Electron temperatures at peak compression of between 200 and 400 eV are indicated. A double channel instrument is currently in use and is shown in Figure 5. This instrument monitors simultaneously the transmission through two foils of the same material but with different thicknesses, or two foils of different material, and thereby gives a time-resolved measure of T_e. Preliminary results with this instrument confirm the above electron temperatures.

4.2 X-ray Crystal Spectrometer

In order to make a more precise study of the X-ray spectrum a crystal spectrometer is at present being manufactured. X-ray crystal analysis of the Scylla spectrum (12) has shown the valuable results of which such an instrument is capable. Schematic drawings of the instrument are shown in Figures 6 and 7. The crystal is mounted on a precision turntable which can be adjusted to 10 s of arc and the 2:1 relationship between angular movement of the turntable and the detector is maintained by epicyclic gears connected by steel tape. Figure 6 shows the system used with a plane crystal in which Soller slits are employed to define the entrance and acceptor beams. An Allen-type photomultiplier is the detector in this arrangement. Alternatively (Figure 7) the instrument can be used with a curved crystal in the focussing mode which is suitable for recording the X-ray spectrum on emulsion.

4.3 Grazing Incidence Spectrograph

The grazing incidence spectrograph shown in Figure 8 uses the conventional optical layout. It is designed to record on plates, but also has provision for photomultipliers. A 2 metre glass grating having 600 lines/mm is used. The provision of 2 alternative entrance slits enables angles of incidence of 86° or 89° to be used, and it is hoped to cover the wave-length range from 1000 Å down to 12 Å with a reciprocal dispersion varying from 3 Å/mm to 0.5 Å/mm. The Rowland Circle is in the vertical plane, and a removable cassette-type plateholder is used which is constructed to a tolerance of 1/5000 in. This instrument is completed and is in the process of being aligned.

4.4 Time-resolved Normal Incidence Spectrograph

The layout of this instrument (14) is shown in Figure 9. It uses a 1 metre 1200 lines/mm grating in a Rowland Circle mounting and records photographically from 500 Å to 2500 Å with a reciprocal dispersion of 8 Å/mm. The spectrum is time resolved by reflection from a rotating mirror at 70° incidence, placed 25 cm from the plate. At a rotor speed of 1000 revs/s, the writing speed is 3 mm/μs with a total writing time of 8 μs. To maintain a stigmatic image the spectrum is recorded at around zero diffraction angle, and the crossed entrance slits are split into vertical and horizontal components, separated along the optic axis. The wave-length range is changed by moving the vertical slit around the Rowland circle and the horizontal slit along a tangent to the Rowland circle.

The first application of this instrument has been to study the emission spectrum of the θ-pinch. Figures 10 and 11 show typical spectrograms taken with Kodak Pathe SC5 film which is sufficiently sensitive to yield a good record from a single exposure. Each spectrogram records over a range of 1000 Å within the wave-length limits of the instrument. The first 20 - 30 μs of each discharge have been recorded with a time-resolution better than 0.5 μs and the successive bursts of continuum and line emission (note particularly the carbon impurity lines) correspond to successive half-cycles of the driving field.

Figure 10 shows a spectrum of a discharge in deuterium at an initial pressure of 300μ. Ionized lines of carbon, nitrogen and oxygen impurities can be seen, the most highly ionized state identified being the $2s\,^3S$ - $2p\,^3P$ triplet of OVII predicted by Edlén (15)

at wave-lengths of 1624, 1638 and 1640 Å. This triplet has not previously been recorded photographically although its appearance in a similar discharge, where it was detected using a monochromator, has been reported recently (16). Since the ^3P state lies 561 eV above the ground state of OVII the appearance of the triplet is supporting evidence for the electron temperatures quoted above. The time of appearance of the triplet is similar to that of the soft X-radiation whilst the variation in intensity of the ionized oxygen lines from OIV to OVII confirms that the electron temperature approaches its maximum at about peak driving field on the second half-cycle. Also of interest is the simultaneous appearance of the isoelectronic doublets, 2^2S - 2^2P, of CIV, NV and OVI. A blend at 2070 Å has been tentatively identified as the (5 - 6) lines of CVI.

The effect of adding 20% of oxygen to the deuterium gas is shown in Figure 11. The most highly ionized states i.e., OVII, CVI and CV no longer appear, indicating that the electron temperature is reduced, whereas lines of Al III and Si IV from the recrystallized alumina discharge tube build up strongly in the later half-cycles.

5. CONCLUSION

Since the electron temperatures produced in the θ-pinch result from a balance between rapid resistive heating by reversed field diffusion and cooling by radiation at wave-lengths below 500 Å it is possible to achieve a wide variety of plasma conditions by control of the impurity content and specification of the sign and amplitude of initial trapped magnetic field. The above discussion has outlined the main features of the radiation from such a hot dense plasma and described briefly the AWRE instruments designed to study them. These instruments are being used to develop spectroscopic methods of determining the particle densities and temperatures, and to analyse the various ionization and recombination processes that lead to the steady state.

REFERENCES

1. K. Boyer et al.: "Studies of Plasma Heated in a Fast-Rising Axial Magnetic Field (Scylla)". Phys. Rev., 119, 831 (1960).

2. H. R. Griem et al.: "Measurements of Electron Densities and Temperatures and other Plasma Parameters in Magnetic Compression Experiments". Salzburg Conference on Controlled Nuclear Fusion Research (1961).

3. A. C. Kolb et al.: "A High Energy Magnetic Compression Experiment". Salzburg Conference on Controlled Nuclear Fusion Research (1961).

4. R. v. d. R. Woolley and D. W. N. Stibbs: "The Outer Layers of a Star". Oxford (1953).

5. G. Elwert, Zeitschrift für Naturforschung: 7a, 432 (1952).

6. W. Finkelnburg and T. Peters: "Handbuch Der Physik". 28, 79 (1957).

7. F. C. Jahoda et al.: Phys. Rev., 119, 843 (1960).

8. T. F. Stratton: Chapter in: "Optical Spectrometric Measurements of High Temperatures". Ed. P. J. Dickerman, Chicago Univ. Press (1961).

9. A. J. Bearden et al.: "X-ray Continua and Line Spectra from Highly Stripped Atoms in a Magnetically Compressed Plasma". Phys. Rev. Letters, 6, 257 (1961).

10. G. Knorr: Zeitschrift für Naturforschung 13a, 441 (1958).

11. R. F. Post: "Impurity Radiation Losses from a High Temperature Plasma". J. Nuc. Energy Part C, 3, 273 (1961).

12. F. L. Ribe et al.: "X-ray Spectroscopic Measurements of High-Temperature Plasma". Proceedings of the Vth International Conference on Ionization Phenomena in Gases, Munich (1961).

13. A. Unsold: "Physik Der Sternatmosphären". Berlin, Springer.

14. A. H. Gabriel and W. A. Waller (to be published).

15. B. Edlén: Arkiv für Fysik, 4, 441 (1952).

16. F. C. Jahoda et al: Phys. Rev., 119, 843 (1960).

SCHEMATIC DIAGRAM OF MAGGI I EXPERIMENTAL SYSTEM

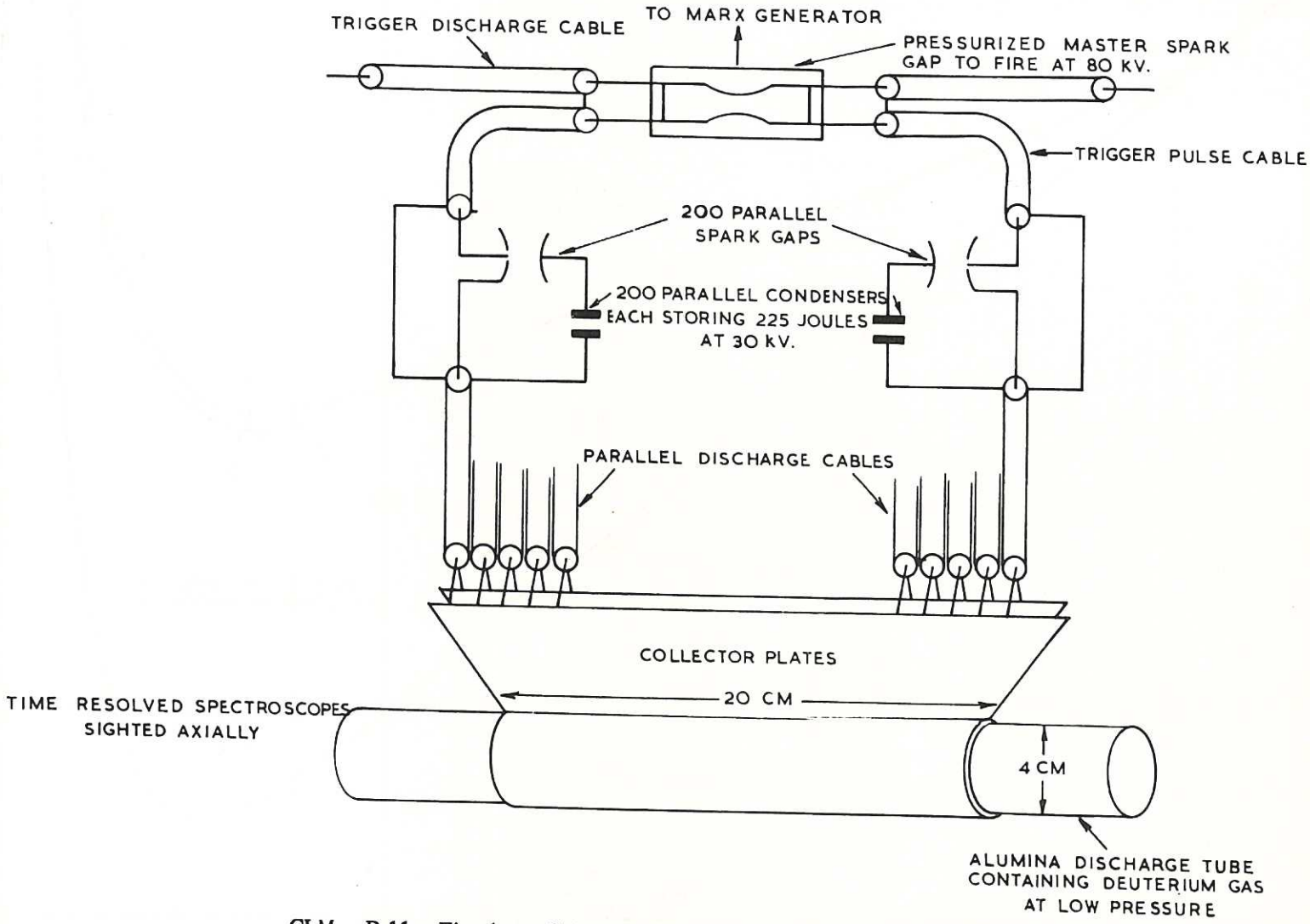

CLM – P 11 Fig. 1 Schematic Diagram of Maggi I Experimental System.

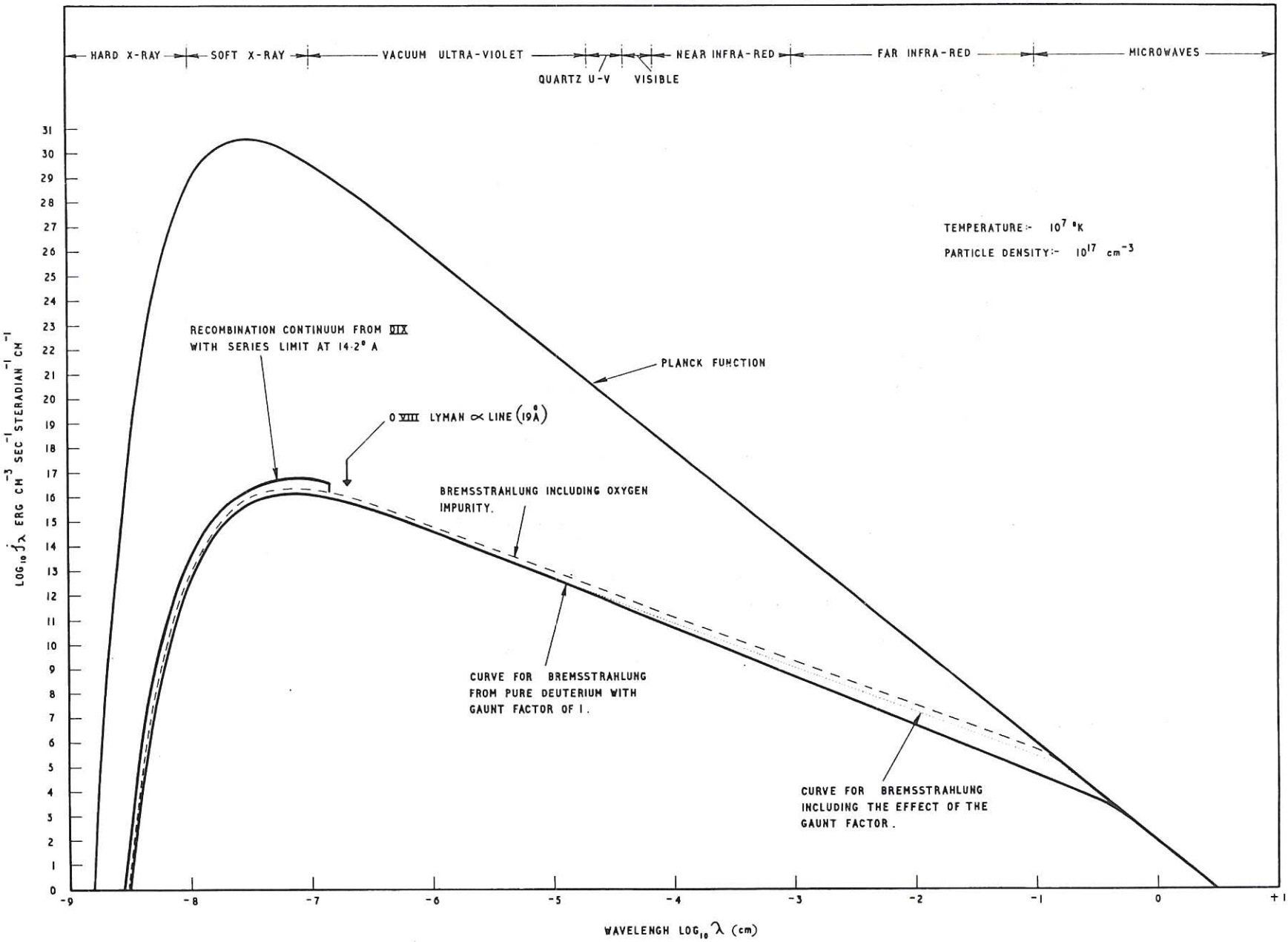

CLM – P 11 Fig. 2 Radiation Spectrum from One Cubic Centimeter of Deuterium Plasma Containing 1% Oxygen Impurity. Temperature 10 ^{o}K and Particle Density 10^{17} cm^{-3}.

X-RAY EMISSION VIEWED THROUGH AXIAL PIN-HOLE CAMERA. DEUTERIUM PRESSURE = 100μ Hg (NO PREIONISATION)

PIN-HOLE PHOTOGRAPHS

EDGE OF FILM CORRESPONDS TO INTERNAL DIAMETER OF DISCHARGE TUBE AT THE MEDIAN PLANE OF THE DRIVING COIL WHICH IS SHOWN AS THE OUTER RING

4 DISCHARGES
PLASMA SCREENED BY
585 $\mu g/cm^2$ CH_2 + 50 $\mu g/cm^2$ Al

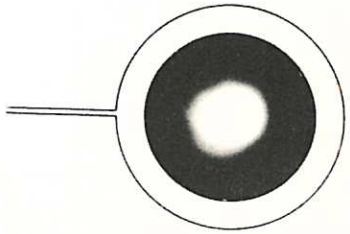

1 DISCHARGE
PLASMA SCREENED BY
585 $\mu g/cm^2$ CH_2 + 50 $\mu g/cm^2$ Al

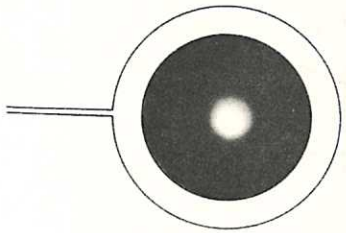

32 DISCHARGES
PLASMA SCREENED BY
923 $\mu g/cm^2$ Al

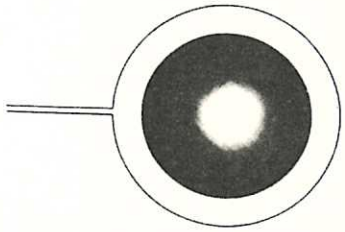

TIME DEPENDENCE OF X-RAY EMISSION

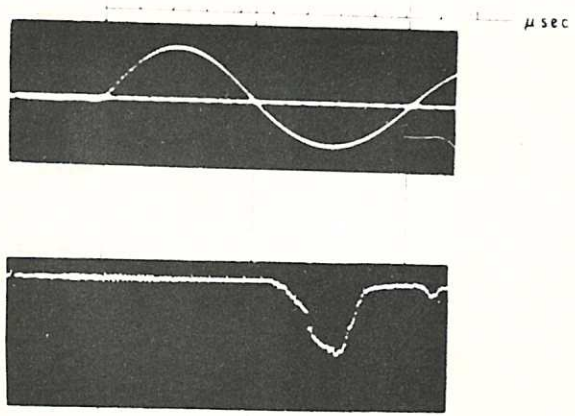

CLM - P 11 Fig. 3 X-ray Emission Viewed through Axial Pin-Hole Camera.

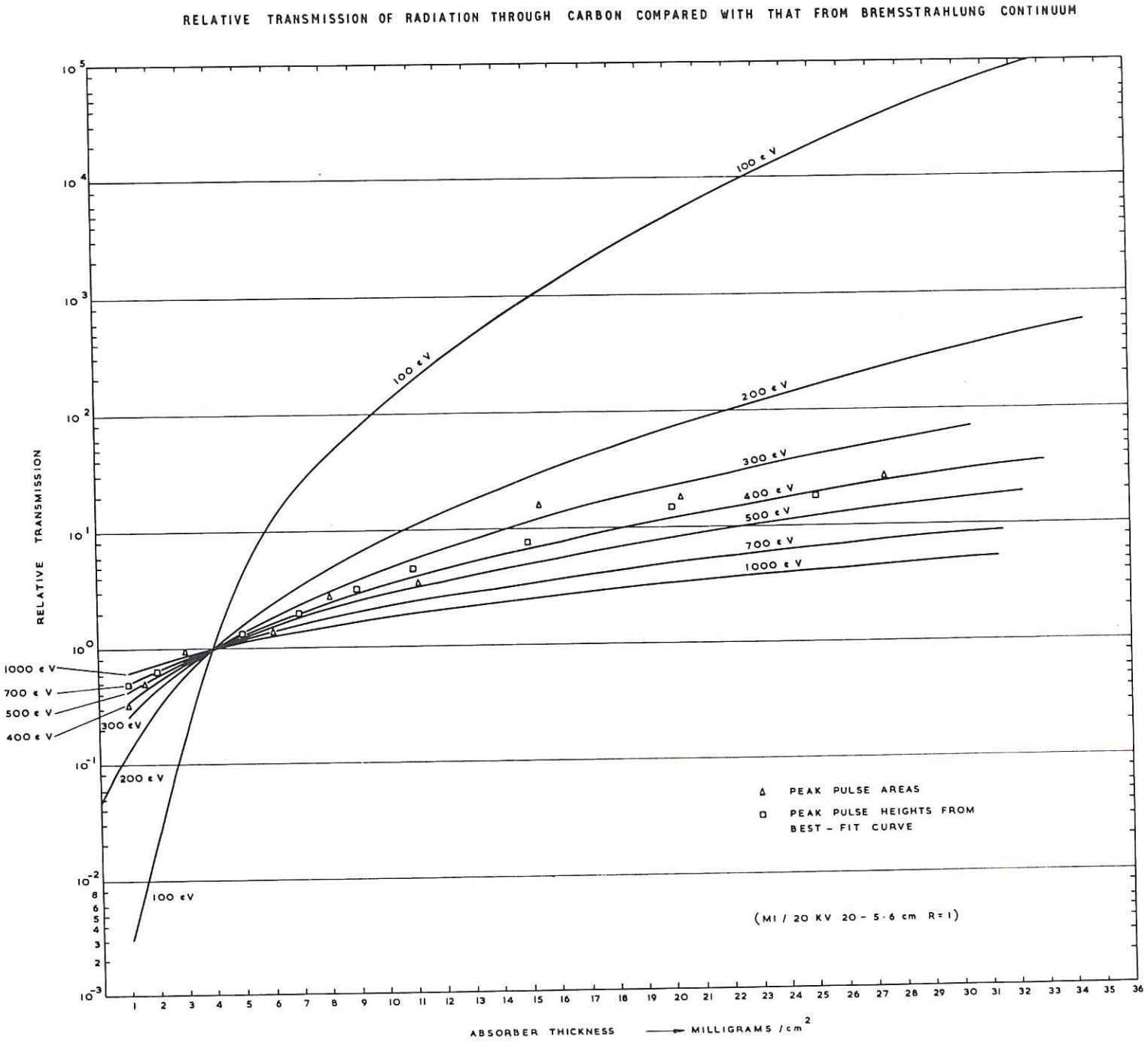

CLM – P 11 Fig. 4 Relative Transmission of Radiation through Carbon Compared with that for Bremsstrahlung Continuum.

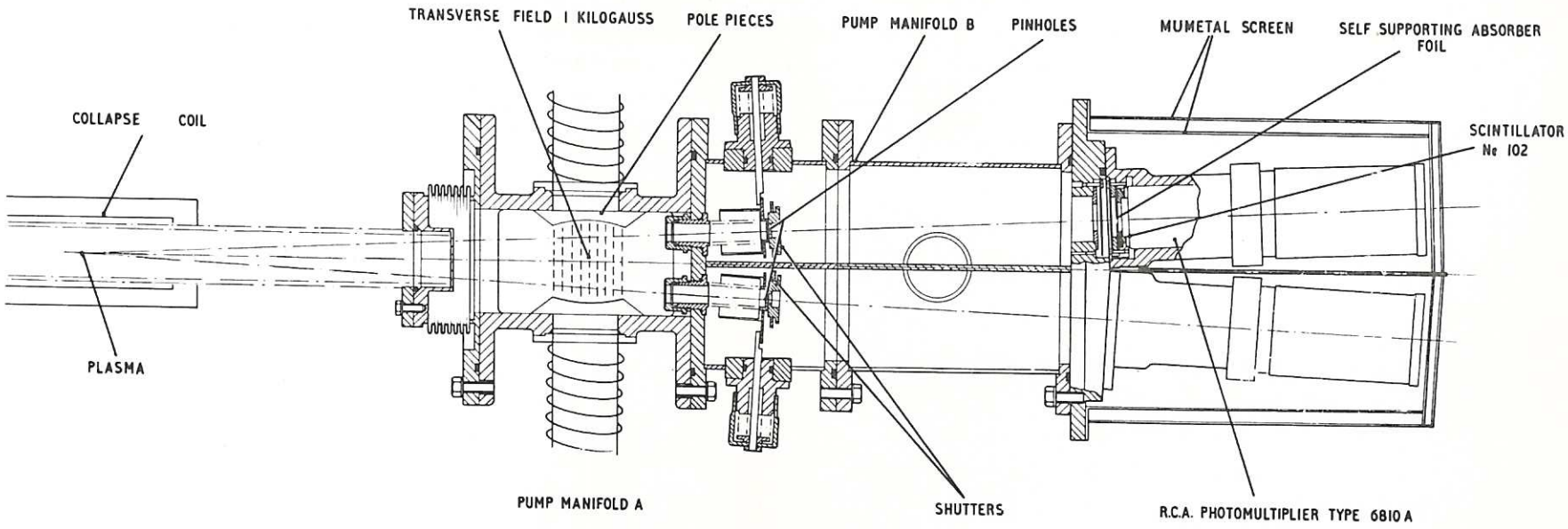

CLM – P 11 Fig. 5 Double Channel X–ray Detector.

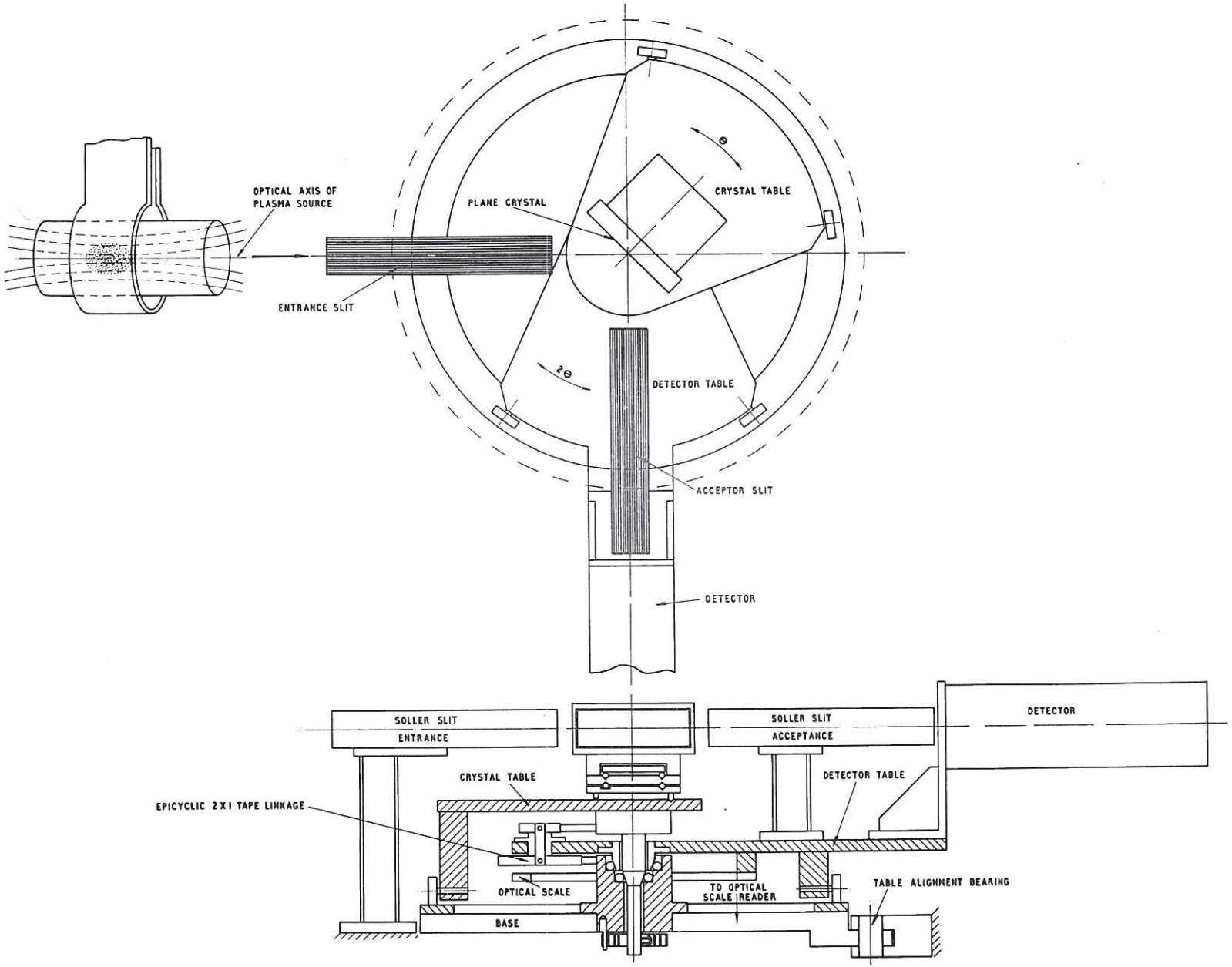

CLM – P 11 Fig.6 Crystal X–ray Spectrometer. Arrangement 1 (Plain Crystal)

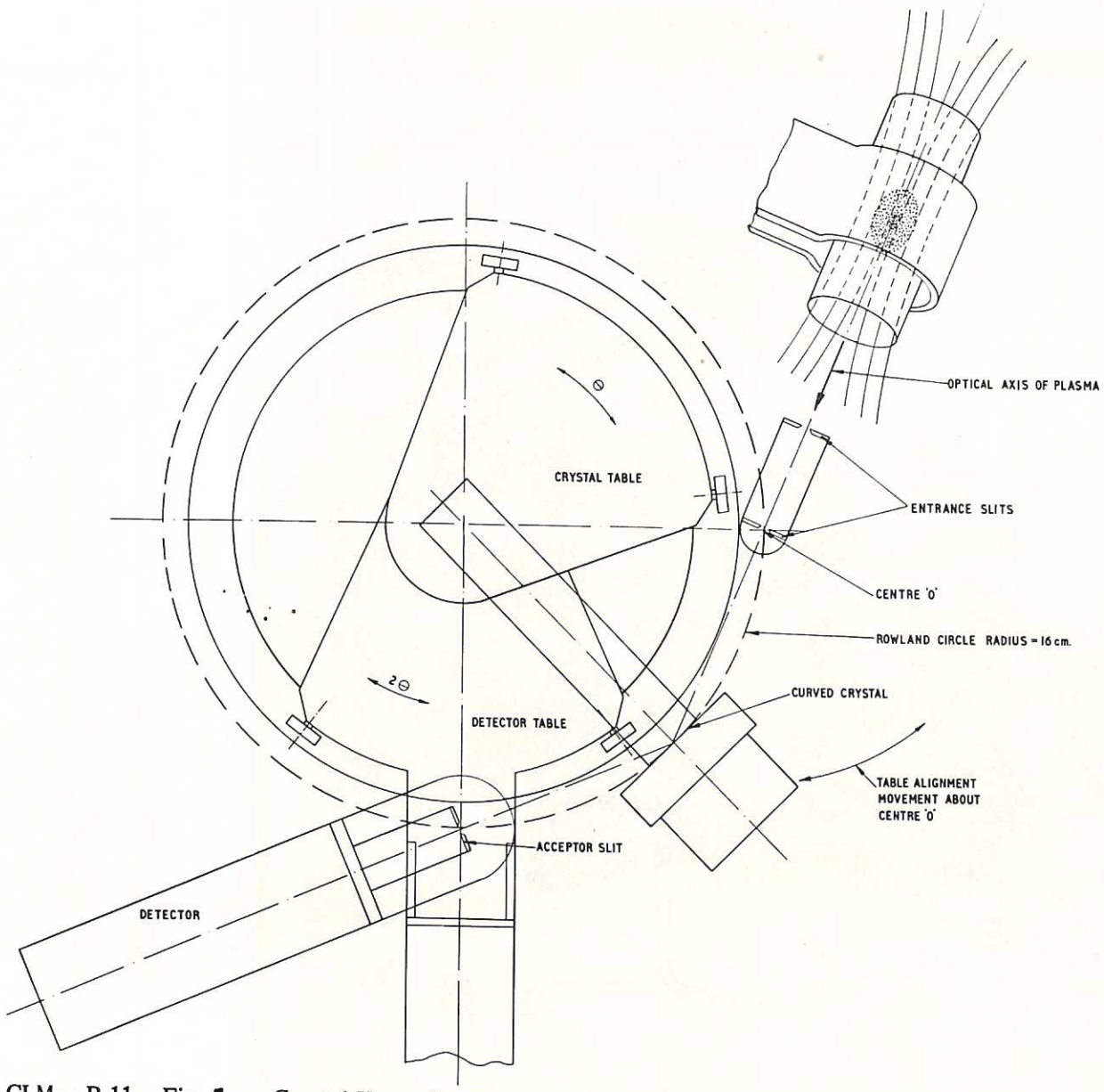

CLM – P 11 Fig. 7 Crystal X–ray Spectrometer. Arrangement 2 (Curved Crystal).

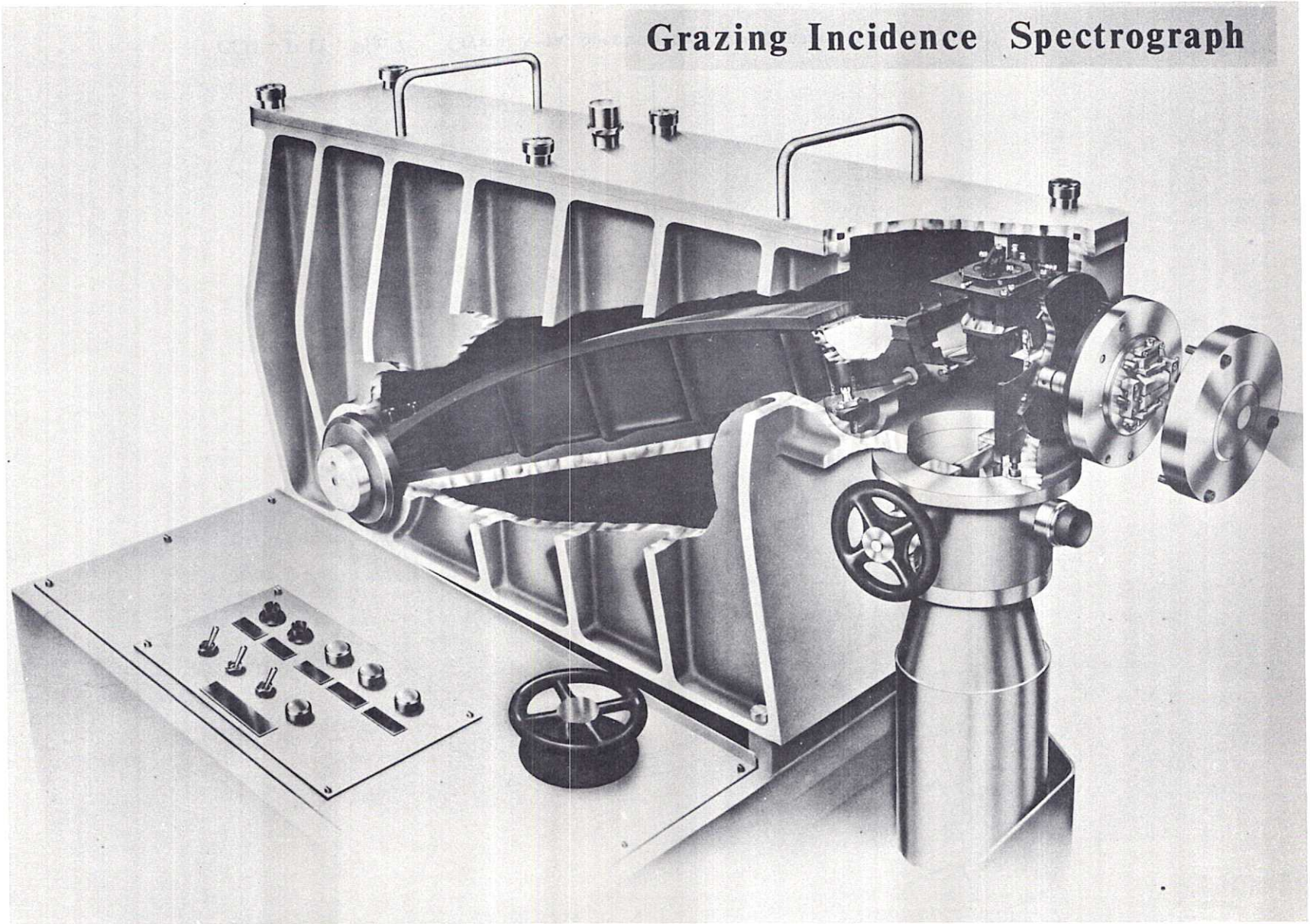

CLM – P11 Fig. 8 Grazing Incidence Spectrograph.

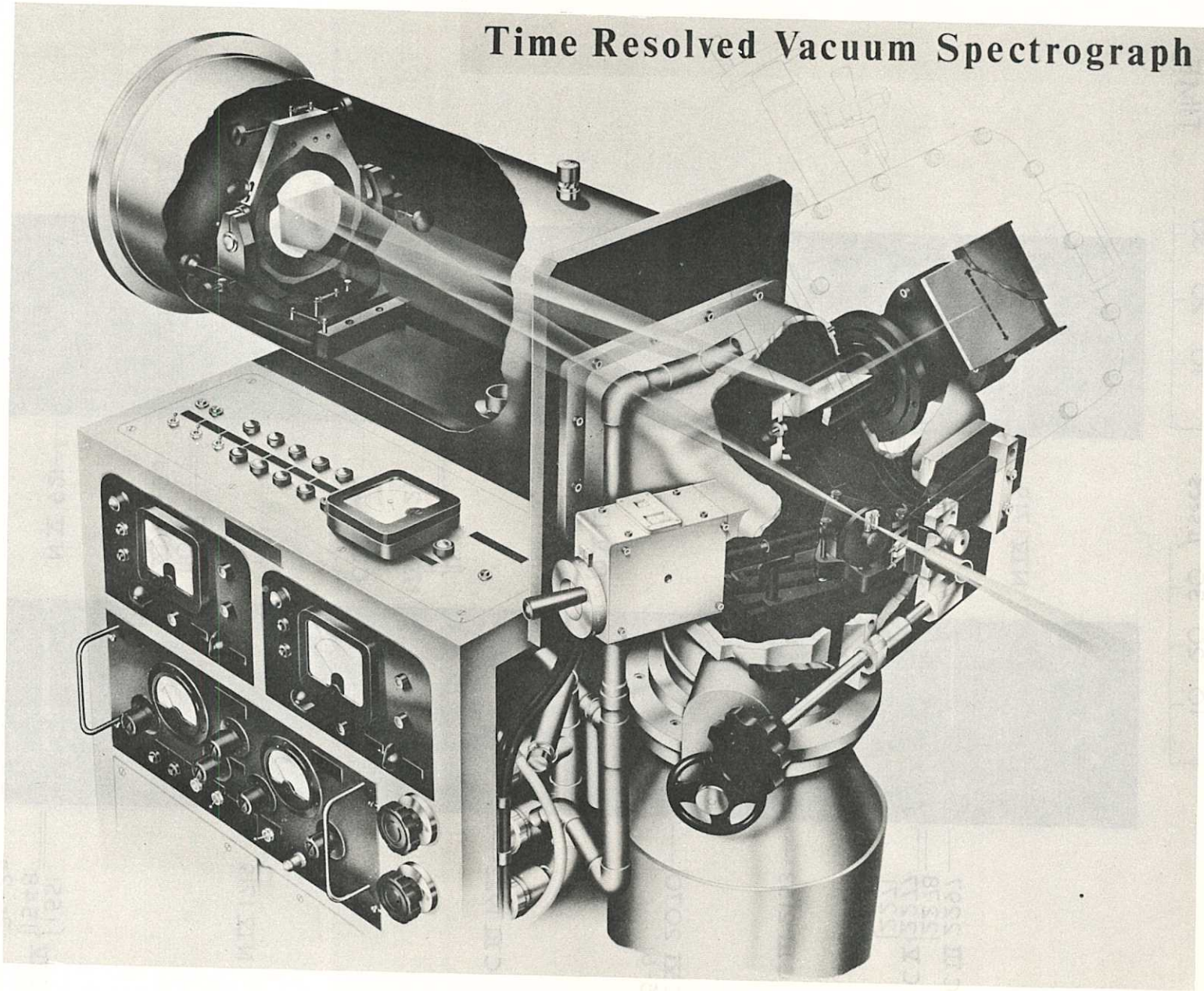

CLM – P 11 Fig. 9 Time–Resolved Vacuum Spectrograph.

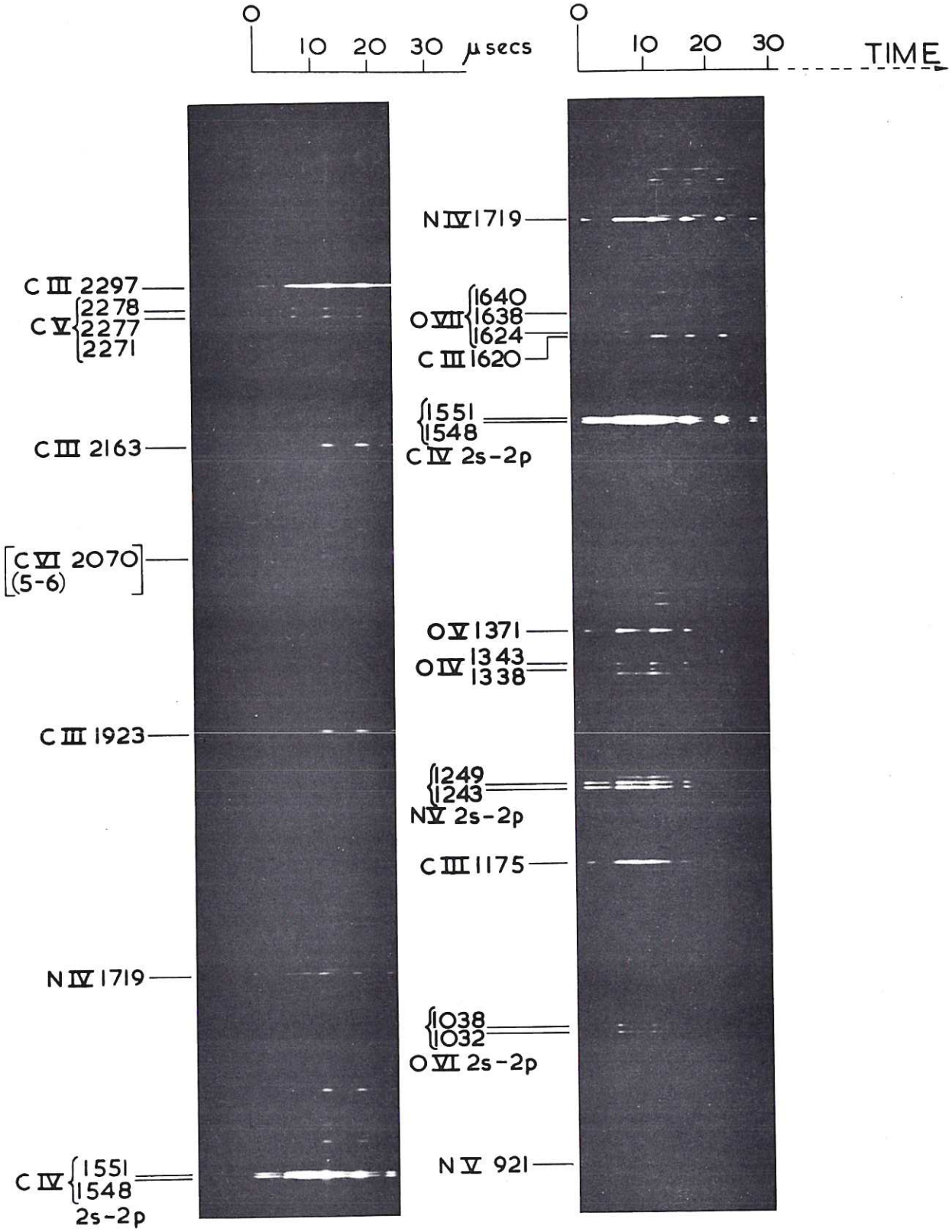

CLM – P 11 Fig. 10 Time–Resolved Spectrogram of Theta–Pinch in Alumina Discharge Tube. Gas is deuterium at 300 μ Hg.

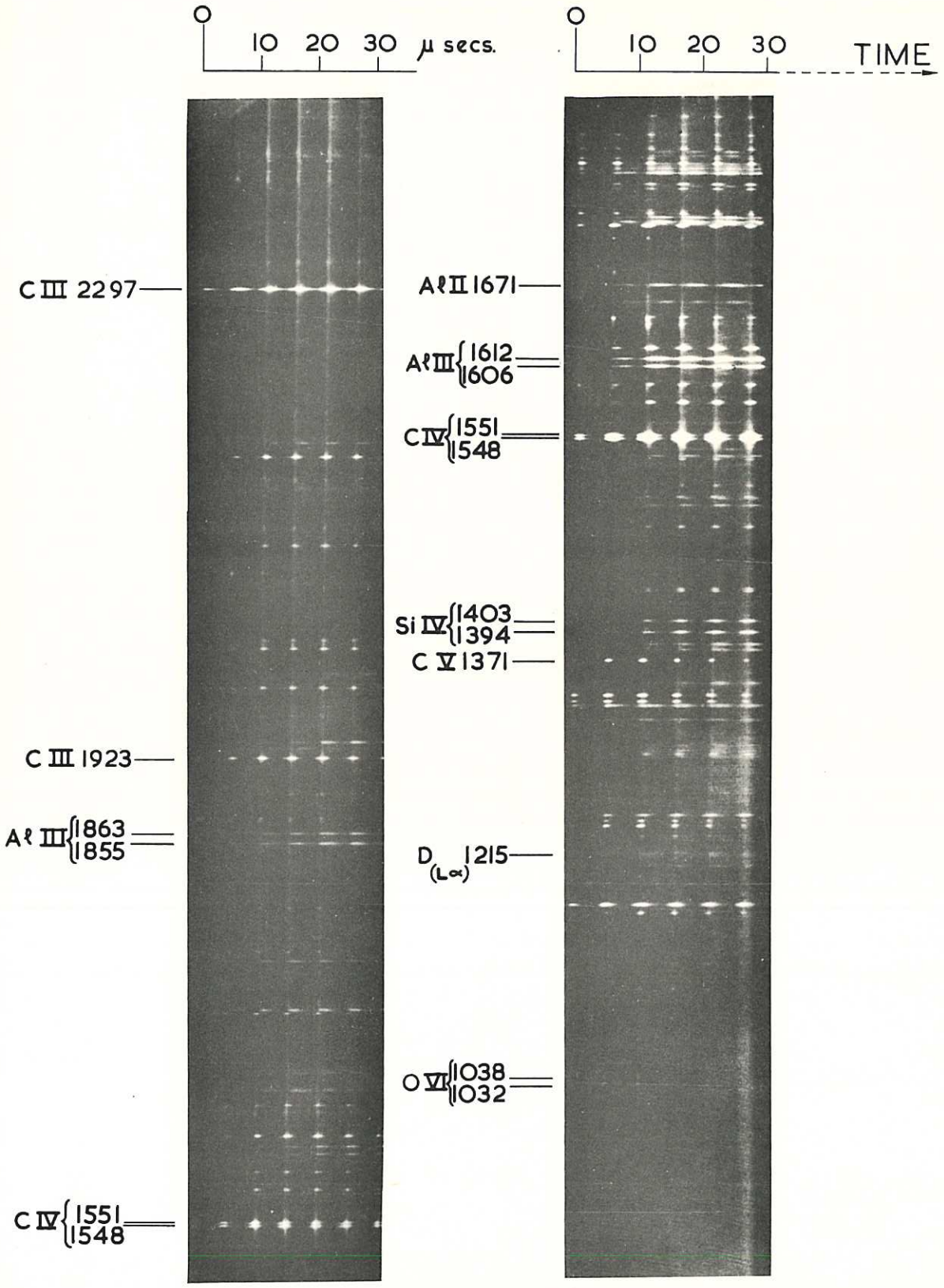

CLM – P 11 Fig. 11 Time–Resolved Spectrogram of Theta–Pinch in Alumina Discharge Tube. Gas is deuterium with 20% added oxygen at total pressure of 300 μ Hg.